Climate Dynamics (2021) 57:757–773
https://doi.org/10.1007/s00382-021-05740-w

Influence of projected climate change, urban development and heat adaptation strategies on end of twenty-first century urban boundary layers across the Conterminous US

Aldo Brandi[1,2] · Ashley M. Broadbent[1,2] · E. Scott Krayenhoff[3] · Matei Georgescu[1,2,4]

Received: 3 September 2020 / Accepted: 16 March 2021 / Published online: 2 April 2021

Abstract

The urban environment directly influences Urban Boundary Layer (UBL) dynamics. Commonly proposed heat adaptation strategies focused on reducing the impacts of global change and urban induced warming are also expected to decrease the intensity of convective mixing thereby reducing UBL depth, with important consequences for air pollutant dilution and dispersion. We use 20-km grid spacing Regional Climate Model decadal scale simulations that account for end of twenty-first century greenhouse gas emissions, urban development and intensive and uniform implementation of a suite of heat adaptation strategies, to investigate the individual and combined impacts of such drivers on UBL dynamics over the Continental US (CONUS). Results indicate that combined impacts of climate change and urban development are expected to increase summer (JJA) daytime UBL height in the eastern CONUS. Heat adaptation strategies lead to a summer daytime UBL depth reduction of several hundred meters across CONUS regions, primarily as a consequence of reduced surface sensible heat fluxes and associated turbulence. Our results confirm that heat adaptation is expected to increase the static stability of both daytime and nighttime UBLs and decrease the magnitude of vertical winds, inducing stronger subsidence. In addition, the large geographical scale of our analysis indicates that adaptation impacts are greater inland and smaller over coastal cities. In Southern California, the adaptation induced increase in latent heat can counterbalance the projected decrease in UBL depth. Future work addressing these projected UBL impacts with convection permitting, high-resolution coupled atmosphere-chemistry simulations is needed to explicitly determine potential unintended consequences for urban air quality.

Keywords Climate change · Urban development · Heat adaptation · UBL · Unintended consequences

1 Introduction

The planetary boundary layer (PBL) is the link between the landscape and its biogeophysical characteristics and atmospheric processes (Pielke and Avissar 1990). The PBL is the lowest part of the troposphere and it experiences a dynamic diurnal cycle of moisture, thermal and scalar (e.g., various pollutants) variability. The diurnally varying structure of the PBL, including its depth, is directly influenced by surface-based forcing to which it responds on timescales of one hour or less (Stull 2012). The atmospheric response to terrestrial variability in albedo, water content and roughness are turbulent processes generated by thermal convection, evapotranspiration and wind shear. Turbulence has a fundamental role in vertical transport and mixing within the boundary layer. Hence, accurate characterization of its evolution has important implications for air quality, shallow and

✉ Matei Georgescu
Matei.Georgescu@asu.edu

Aldo Brandi
abrandi@asu.edu

[1] School of Geographical Sciences and Urban Planning, Arizona State University, 975 S. Myrtle Ave., Fifth Floor, Tempe, AZ 85287-5302, USA

[2] Urban Climate Research Center, Arizona State University, Tempe, AZ 85287, USA

[3] School of Environmental Sciences, University of Guelph, Guelph, ON N1G 2W1, Canada

[4] Global Institute of Sustainability, Arizona State University, Tempe, AZ 85287, USA

deep convection, and cloud formation (Weaver and Avissar 2001; Pielke 2001; Seidel et al. 2012).

The depth of the PBL can be identified as the altitude of potential temperature and mixing ratio inversions within the mixed layer or as the height where surface-driven turbulence production ceases (Stull 2012). Two ways to make such an assessment are direct measurements of meteorological variables, including wind speed and potential temperature, and numerical modeling (Seibert et al. 2000). Meteorological variables can be measured in situ, through instrumented towers, tethered balloons, radiosondes and aircrafts or remotely sensed with sonar, radar and lidar technologies. However, these measurements are usually spatially and temporally limited to specific campaigns or particular locations and are not available for long-term analysis over broad spatial extents. Thus, mesoscale climatological research often relies on numerical models to determine boundary layer characteristics, which are commonly parameterized through schemes that use threshold "critical" values of the turbulent kinetic energy (TKE) equation or of the Richardson number (Ri), defined as the ratio between the buoyancy and shear production terms of the TKE budget (Zhang et al. 2020).

The evolution of the PBL over urban environments is altered by a landscape that is characterized by an abundance of paved impervious surfaces, anthropogenic heat sources, and three-dimensional building morphology. These characteristics of urban environments are at the foundation of the urban heat island (UHI) effect, defined as the difference in air (or surface) temperatures between the city and the surrounding unbuilt areas (Oke 1982). Consequently, urban boundary layers (UBLs) are markedly different from their rural counterparts, as augmented roughness and sensible heat fluxes lead to deeper and stronger mixing (Barlow 2014). Characterizing the evolution of UBLs is of particular importance since most human activities occur within this lowest portion of our atmosphere, generally within 1–3 km above the surface.

Combined impacts of a warming climate and urban development (here defined as the combination of urban expansion and densification) are increasing the intensity and frequency of extreme heat events (Meehl and Tebaldi 2004; Krayenhoff et al. 2018; Broadbent et al. 2020b). As a consequence, heat adaptation has become a pressing priority for many cities, especially in the US and Europe (Synnefa et al. 2008; Gilbert et al. 2016; Aleksandrowicz et al. 2017; Wang et al. 2019; Bruinsel 2020). Commonly utilized thermal adaptation approaches achieve their objectives via modification of urban landscape properties (Krayenhoff et al. 2021). Examples range from cool roofs and other reflective surfaces that reduce heat absorption of buildings and pavements by increasing surface albedo (Akbari and Matthews 2012), to green and evaporative roofs that increase the latent fraction of turbulent heat flux partitioning through evapotranspiration processes of plants (Bass et al. 2003). Some strategies, like street trees, provide shade over paved surfaces, reducing surface-absorbed solar energy while also permitting evapotranspiration (Gillner et al. 2015).

The desired outcome associated with heat adaptation strategies is the lowering of urban temperatures at the surface. However, the modified land cover and its repartitioning of turbulent fluxes may lead to unintended consequences. For example, reducing the amount of sensible heat flux arising from the surface decreases the potential temperature lapse rate in the lower atmosphere, in turn decreasing vertical mixing and the overall depth of the UBL, with implications for pollutant dilution and dispersion (Zilitinkevich 2012; Georgescu 2015; Sharma et al. 2016; Song and Wang 2016). Several studies have addressed the unintended consequences associated with the aforementioned heat adaptation strategies. Sailor (1995) demonstrated, using a modified version of the Colorado State University Mesoscale Model, that cool and green roofs can lower the PBL depth by 50 m over the Los Angeles basin. Using the Weather Research and Forecasting (WRF) mesoscale model, Zhang et al. (2017) showed that cool and green roofs decreased temperatures, increased stability and reduced the height of UBLs during the summer of 2013 across the Yangtze River Delta region. Georgescu (2015) used the WRF model to show that roofing technologies are expected to lead to a reduction in TKE in a projected 2100 urban development scenario across California. Similarly, Song et al. (2018) and Chen and Zhang (2018) used WRF simulations to estimate reductions of UBL depth, CAPE and TKE over the Phoenix and the Suzhou–Wuxi–Changzhou metropolitan areas, respectively. All of these studies agree on the UBL depth reduction and convective mixing suppression potential of heat adaptation strategies.

Studies that explicitly investigate the impact of street trees on the UBL are rather scarce. Using an offline single layer urban canopy model, Song and Wang (2016) examined the effect of multiple adaptation strategies and showed that urban greening (cool and green roofs and street trees) reduced the depth of the daytime convective boundary layer but increased that of the nighttime stable boundary layer over Phoenix, AZ. Using in situ measurements in the city of Tokyo, Japan, Narita et al. (2008) highlighted the modulating role of tree crowns in trapping nighttime ground emitted longwave radiation at street level. They found that nighttime radiative cooling was hindered by tree crowns, leading to road surface temperatures being 1.5 °C higher than streets with no trees. To improve process-based understanding associated with tree deployment as an urban thermal adaptation strategy, Krayenhoff et al. (2020) developed a neighborhood-scale multi-layer urban canopy model that explicitly includes the radiative effects of trees. Further development of such tools including their coupling with mesoscale models that

represent dynamics, surface energy balance and hydrology impacts is expected to advance fundamental understanding associated with multi-scale urban greening efforts across urban agglomerations, including implications for the structural evolution of the UBL.

To our knowledge, there is no published assessment of the impact of climate change on UBL depth. Here we build on previous work to investigate the potential impacts associated with explicit representation of end of twenty-first century greenhouse gas induced climate change and urban development, including heat adaptation strategies, on UBLs across broad geographical scales (i.e., the Continental US). We perform a detailed comparison of UBL dynamics across a range of climatic regions and cities. We consider several heat adaptation measures and assess their impacts on UBL both individually and simultaneously, and we pair such assessment to the analysis of changes in surface energy balance drivers. We use decadal scale WRF simulations of a suite of contemporary and projected futures across the continental US (CONUS) to investigate the combined impacts of greenhouse gas induced climate change, urban development, and heat adaptation strategies on UBL depth and structure. We provide a climatological assessment of the diurnal, seasonal and annual UBL impacts associated with heat adaptation in urban environments, focusing on a large geographical domain.

2 Methods

2.1 Model description and PBL parameterization scheme

The Weather Research and Forecasting (WRF) model is a mesoscale weather prediction tool that enables assessment of land–atmosphere interactions across a continuum of spatial scales. WRF has been extensively used for a variety of different meteorological and climatological applications (e.g., Chen et al. 2011; Xue et al. 2014). We use the Advanced Research Version (ARW) of WRF (version 3.6; Skamarock et al. 2008) coupled with a single layer urban canopy model (SLUCM; Kusaka et al. 2001; Kusaka and Kimura 2004). The SLUCM represents built-up areas as a symmetrical street canyon of infinite length and simulates energy, momentum and water exchange between the urban surface and overlying atmosphere. An urban grid cell is fractionally divided into pervious and impervious components. The SLUCM represents physical processes occurring within the impervious portion of the urban grid cell (e.g., building shadowing, anthropogenic heating) while the Noah land surface model (LSM) accounts for energy, momentum and water exchange between the soil/vegetation (i.e., the pervious component) and the overlying atmosphere (Tewari et al. 2004). The Noah LSM has four soil layers and predicts the moisture and temperature evolution among these layers and between the surface and overlying atmosphere. The Yonsei University (YSU) parameterization scheme is used to represent boundary layer dynamics. The YSU PBL scheme is the evolution of the Hong and Pan (1996) first-order closure non-local vertical diffusion scheme, modified to include a counter-gradient term and an explicit entrainment treatment term in the turbulent flux equation. PBL height, the main focus of this research, is defined as the height within the inversion layer where the entrainment flux is minimum and it is assessed in a two-step process. First, a bulk Richardson number (Rib) is calculated between each model level and the surface level using the following equation:

$$Rib(z) = \frac{g\left[\theta_v(z) - \theta_s\right]z}{\theta_{va}U(z)^2}, \quad (1)$$

where g is gravity acceleration, θ_v is the virtual potential temperature, θ_s is the potential temperature near the surface, θ_{va} is the virtual potential temperature at the lowest level and U(z) is the horizontal wind speed (Hong et al. 2006). Next, this value is compared to a critical bulk Richardson number set equal to zero ($Ri_c = 0$, Noh et al. 2003, Hong et al. 2006). This value of Ri_c is lower than the empiric estimate of 0.25 (Stull 2012) and is expected to highlight the contribution of surface-based buoyancy (i.e., surface-induced heat fluxes, as represented in the numerator of the ratio in Eq. 1) to turbulence production.

2.2 Data and simulations

We analyze a suite of continuous ten-year simulations for contemporary (2000–2009) and projected future (2090–2099) climate conditions, with and without projected urban development (Krayenhoff et al. 2018). The simulation domain covers most of North America with a 20-km horizontal grid spacing centered on the conterminous United States (CONUS) and includes 30 vertical model levels. Simulation output is saved every three hours. Initial and boundary conditions for the contemporary simulations are provided by the European Center for Medium-Range Weather Forecast (ECMWF) 'ERA Interim' reanalysis dataset (Berrisford et al. 2011). Forcing for end-of-century simulations is provided by the Community Earth System Model Coupled Model Intercomparison Project 5 ensemble (CESM CMIP5) RCP 8.5 projections (Monaghan et al. 2014). RCP 8.5 assumes intensive greenhouse gas emissions throughout the twenty-first century (IPCC 2014).

The contemporary and projected representations of urban areas are derived from the Integrated Climate and Land Use Scenarios project (U.S. EPA 2010). The ICLUS project uses population and housing density estimates to produce

semi-decadal downscaled scenarios of urban development consistent with the Intergovernmental Panel on Climate Change (IPCC) Special Report on Emissions Scenarios (SRES, Bierwagen et al. 2010) through 2100. The ICLUS datasets include 1-hectare and 1-km housing density and impervious fraction urban landscape estimates, respectively. These data are aggregated to the 20-km grid spacing WRF domain using a three-tiered urban classification: low density, medium density and commercial/industrial development. ICLUS 2010 is used to represent urban areas across CONUS for the start-of-century simulations, while ICLUS 2100 is utilized to represent the physical expansion of the built environment for end-of-century simulations (Krayenhoff et al. 2018, Supplementary Fig. 15). Comparisons of the two datasets show a ubiquitous increase in urban fraction from ICLUS 2010 to ICLUS 2100, with development values ranging from 10 to 25%. No urban pixel in ICLUS 2010 transitioned to non-urban in ICLUS 2100 (Krayenhoff et al. 2018).

We utilize the A2 SRES ICLUS pathway since it is broadly consistent with RCP 8.5 emission scenarios (Solomon 2007). We incorporate the Moderate Resolution Imaging Spectroradiometer-based 20-category classification for non-urban landscape representation in all simulations.

We examine the climatological effect of a suite of heat adaptation scenarios, including cool roofs, green roofs and street trees. All roofing technologies are uniformly applied across CONUS city roofs to ascertain the maximum potential impact associated with the choice of strategy. For cool roofs, we incorporate a reflectivity of 0.88, the maximum Energy Star Solarflect value after 3 years of deterioration (Energy Star 2013). Green roofs are represented by evaporative roofs operating under the assumption of unlimited water availability. Street trees are parameterized to represent partial solar radiation penetration through the tree canopy, and all solar radiation in the canopy is assumed to be diffuse. In addition, to conserve energy, all intercepted shortwave radiation is converted into water vapor under the assumption of high soil water availability. Longwave radiation effects of trees, which primarily affect the street level and not the UBL, are not accounted for here. Finally, a "Full Adaptation" scenario is implemented consisting of all three previously described strategies applied simultaneously. Table 1 provides a list of all simulations used for the analysis. Additional information on climatological forcing, land cover, urban development scenarios, model settings, and physics schemes utilized, including a comprehensive model evaluation across broad regions as well as across individual cities, can be found in Krayenhoff et al. (2018) and Broadbent et al (2020a).

We largely focus our analysis to summer seasons (JJA) for both start (2000–2009) and end (2090–2099) of the twenty-first century. To quantify the significance of simulated results presented as maps in the regional analysis section (§ 3.1) we utilize pairwise comparisons of individual realizations (Von Storch and Zwiers 2001). Differences between scenarios are first averaged across the summer periods of each year for both start and end of century decades. Next, 10-year averages are calculated and checked for robustness by comparing the sign (positive or negative) of the values in the decadal averages against those in each annual average, pixel by pixel. We define a difference as being significant when the decadal-average difference has the same sign as in 9 (or more) annual-average differences. The probability of such a difference occurring randomly is less than 0.005%. Finally, all non-urban pixels have been masked to highlight the signal arising from the built environment. Results presented as plots and graphs in the city-by-city comparison section (§ 3.2) display the uncertainty as shaded areas or whiskers representing 1σ standard deviation of the 10-year averages.

Table 1 Summary of all WRF simulations used in this study

Simulation no.	Time period	GCM forcing	Urban land cover	Adaptation strategy
1	2000–2009	ECMWF	ICLUS A2 2010	No Adaptation
2	2000–2009	ECMWF	ICLUS A2 2100	No Adaptation
3	2090–2099	CESM (RCP 8.5)	ICLUS A2 2010	No Adaptation
4	2090–2099	CESM (RCP 8.5)	ICLUS A2 2100	No Adaptation
5	2090–2099	CESM (RCP 8.5)	ICLUS A2 2100	Cool roofs
6	2090–2099	CESM (RCP 8.5)	ICLUS A2 2100	Green roofs
7	2090–2099	CESM (RCP 8.5)	ICLUS A2 2100	Street trees
8	2090–2099	CESM (RCP 8.5)	ICLUS A2 2100	Full Adaptation (Cool roofs + Green roofs + Street trees)

3 Results

We first present results as composite maps, showing regional impacts of urban development, climate change and heat adaptation strategies on UBL depth and surface heat fluxes at 14:00 LMST (Local Mean Solar Time) for every urban location across CONUS. We initially focus on this portion of the diurnal cycle because this is the time of day when impacts on UBL depth are typically strongest. Finally, we select eight metropolitan areas for further analysis to facilitate city-by-city comparisons across a suite of municipalities across CONUS (Fig. 1). These municipalities were chosen as they incorporate cities located in different climatic regions and exhibiting different urban development patterns in terms of population and growth rates (Census Regions and Divisions of the United States).

3.1 Regional analysis

The separate and combined impacts of urban development, climate change and heat adaptation strategies on UBL depth are first examined for all of CONUS. We present summertime impacts on UBL depth and surface heat fluxes as temporally averaged differences between scenarios. The effect of urban development on 14:00 LMST UBL JJA height over CONUS shows significant increases of several tens of meters over urbanized areas, with similar impacts under a contemporary and projected future climate (Fig. 2a, d, respectively). Projected changes in 14:00 LMST summertime UBL depth due to urban development are comparable for start-of-century (simulation no. 2 minus simulation no. 1, Table 1; Fig. 2a) and end-of-century (simulation no. 4 minus simulation no. 3, Table 1; Fig. 2d) climates, highlighting similar effects of urban development irrespective of background climate conditions. Exceptions are found in a few locations. For example, in some areas (e.g., Chicago), climate change exacerbates the impact of urban development on UBL height (Fig. 2d). In other parts of CONUS, including urban areas within Texas and Florida, climate change decreases the impact of urban development on summertime UBL depth.

Increases in UBL height due to urban development are driven by increased sensible heat fluxes (Fig. 2b, e) and reduced latent heat fluxes (Fig. 2c, f). The decrease of UBL height over central California resulting from urban development under a start-of-century climate (Fig. 2a) is based on landscape transitioning from primarily agricultural land use at the start of the century to built-up landscapes by the end of the century. Such a transition entails enhanced heat storage within the urban fabric and results in reduced daytime sensible heat flux with correspondingly little change

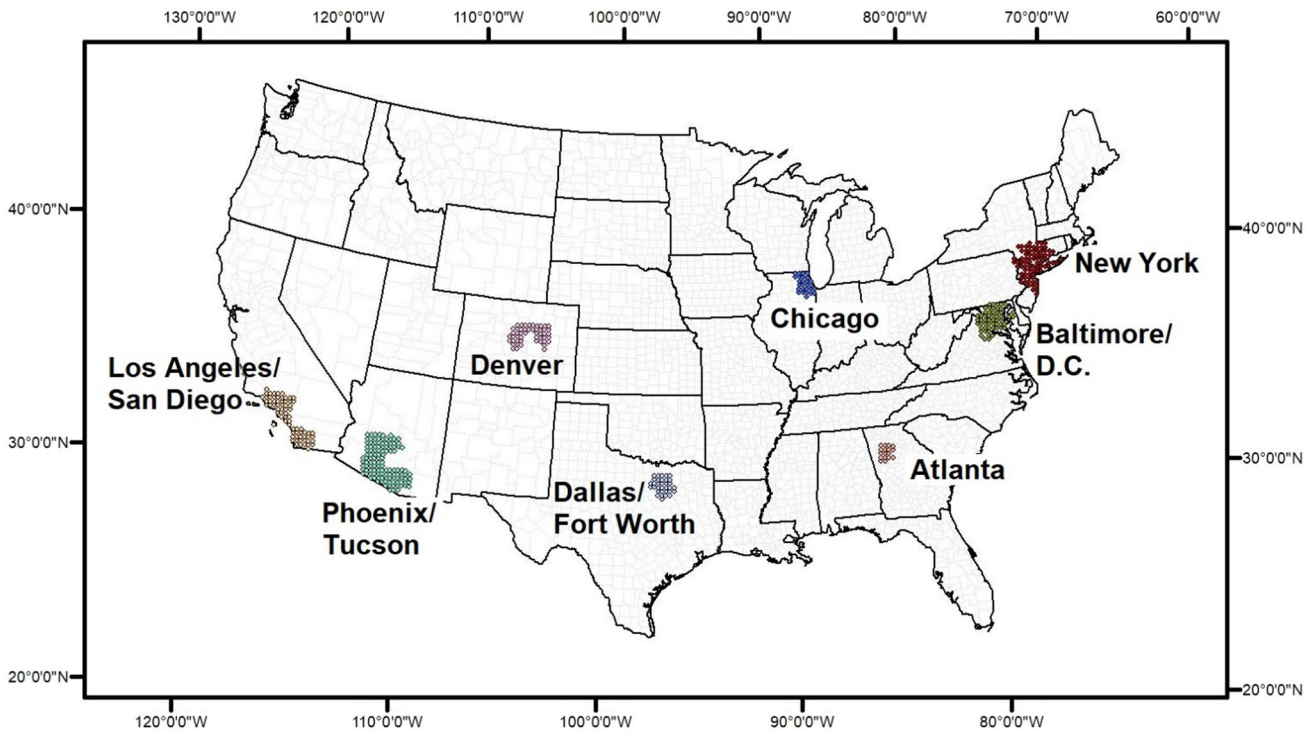

Fig. 1 Geographical map of the Conterminous US, with state borders represented as black solid lines and county lines as gray solid lines. Highlighted in colors are the urban regions/cells considered for metropolitan-level analysis

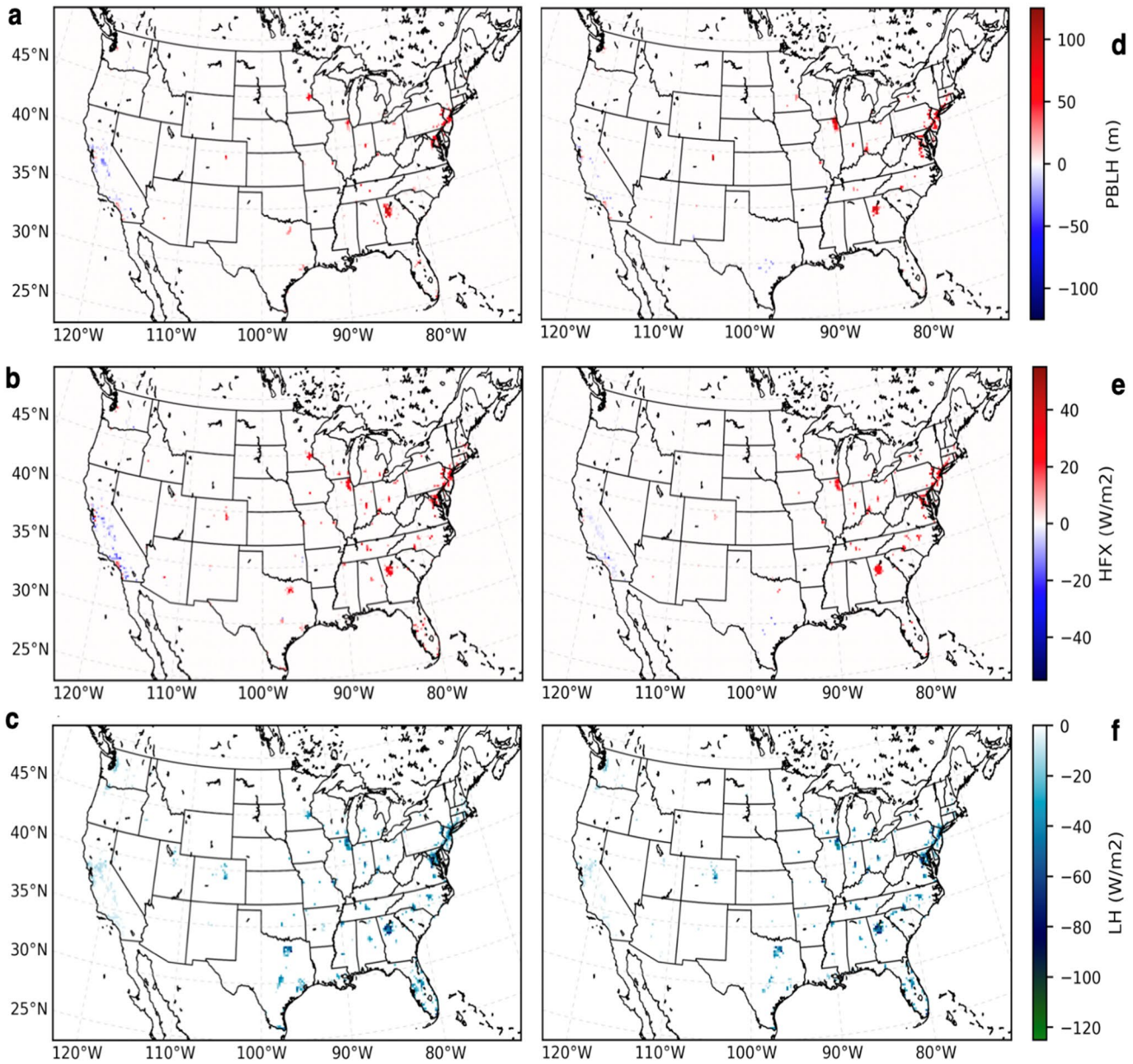

Fig. 2 WRF simulated ten-year averaged summertime (JJA) difference in **a** boundary layer depth, **b** sensible and **c** latent heat flux due to urban development (ICLUS A2 2100—ICLUS 2010) under start of century climate (ECMWF ERA Interim forcing). **d–f** Same as **a–c** but for a projected end of century climate (CESM RCP 8.5 forcing). Results are shown for 14:00 LMST

in daytime near-surface temperatures. These results agree with findings demonstrating the effect of urban development, and consequently, excess heat storage, on daytime 2-m air temperature changes for California and urbanizing regions in China (Georgescu 2015; Cao et al. 2018).

To explore the climatological impacts resulting from a nationwide implementation of heat adaptation strategies across US cities, we next examine the impacts of cool roofs, green roofs and street trees (individually and simultaneously) on UBL depth under a projected future climate (CESM RCP 8.5). Figure 3 shows the JJA impact of cool roofs (simulation no. 5 minus simulation no. 4, Table 1; Fig. 3a), green roofs (simulation no. 6 minus simulation no. 4, Table 1; Fig. 3b) and street trees (simulation no. 7 minus simulation no. 4, Table 1; Fig. 3c) on UBL heights over CONUS in a projected end-of-century climate (CESM RCP 8.5). Results, as before, are shown for 14:00 LMST. Simulation results indicate reductions of UBL heights in the range of tens to hundreds of meters for all heat adaptation strategies considered. The greatest impact arises from the

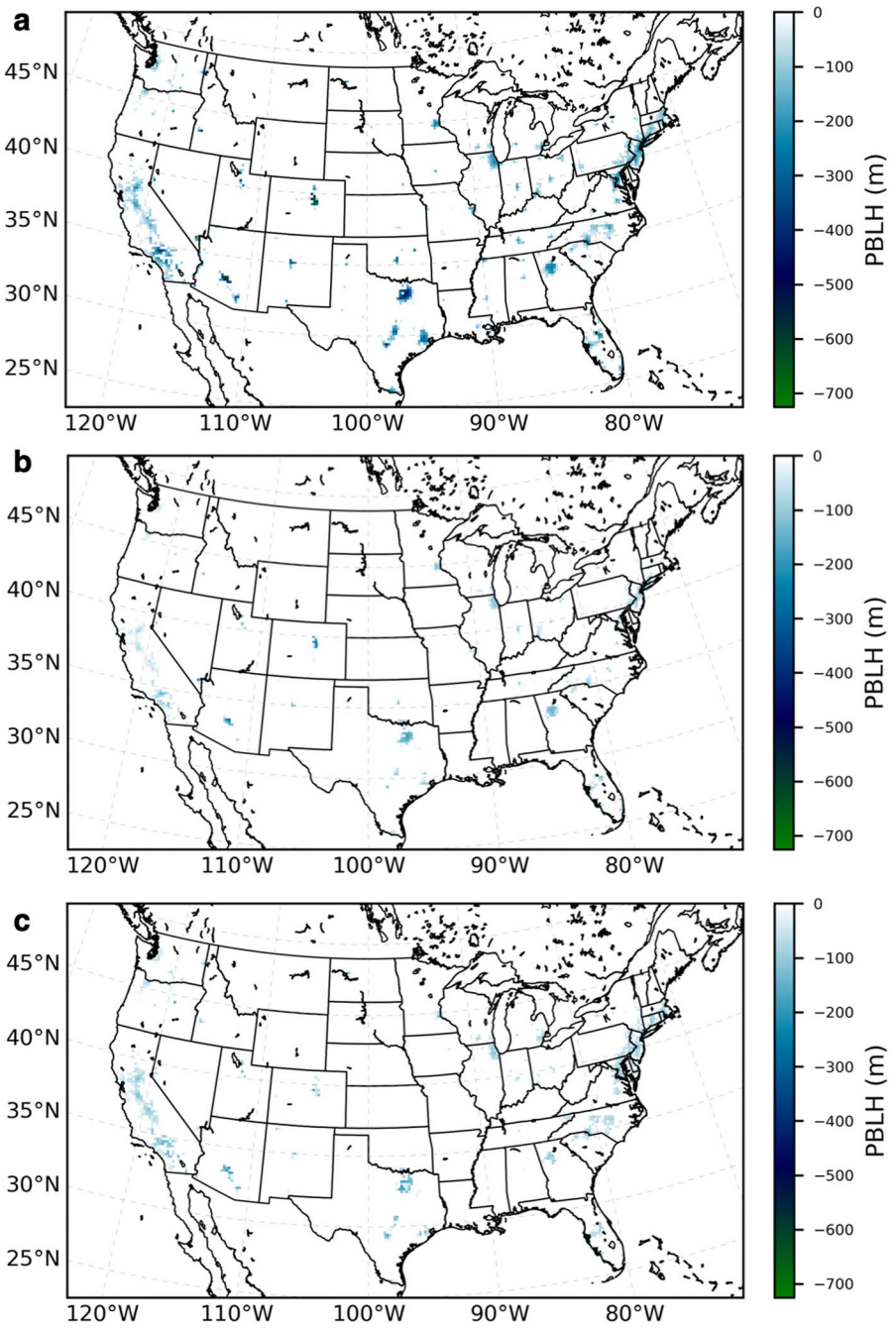

Fig. 3 WRF simulated ten-year averaged summertime (JJA) difference in boundary layer depth resulting from heat adaptation implementation on urban development (ICLUS A2 2100) for a projected end of century climate (CESM RCP 8.5 forcing): **a** Cool roofs, **b** green roofs and **c** street trees. Results are shown for 14:00 LMST

implementation of cool roofs (Fig. 3a), with peak reductions situated over the Phoenix, Denver and Texas metropolitan areas. Green roofs (Fig. 3b) and street trees (Fig. 3c) produce smaller but more uniform reductions throughout CONUS. These results are consistent with those of Krayenhoff et al. (2018) who showed that cool roofs have the highest surface air temperature cooling potential in urban areas affected by urban development and climate change across CONUS and are also consistent with the results of other previous research efforts (e.g., Georgescu et al., 2014; Costanzo et al. 2016). The individual effect owing to each heat adaptation strategy provides a means for geographically explicit impact assessment, highlighting the relative thermal reduction performance among the adaptation choices examined. Similarly, the combined utility of adaptation strategies, incorporating aspects of each, may provide additional insight. Figure 4a shows the impact of simultaneous and uniform deployment of all adaptation strategies (i.e., full adaptation; simulation no. 8 minus simulation no. 4, Table 1) on JJA UBL depth over all CONUS urban areas in a projected end-of-century climate (CESM RCP 8.5) at 14:00 LMST. UBL height is projected to decrease everywhere, with peak change values

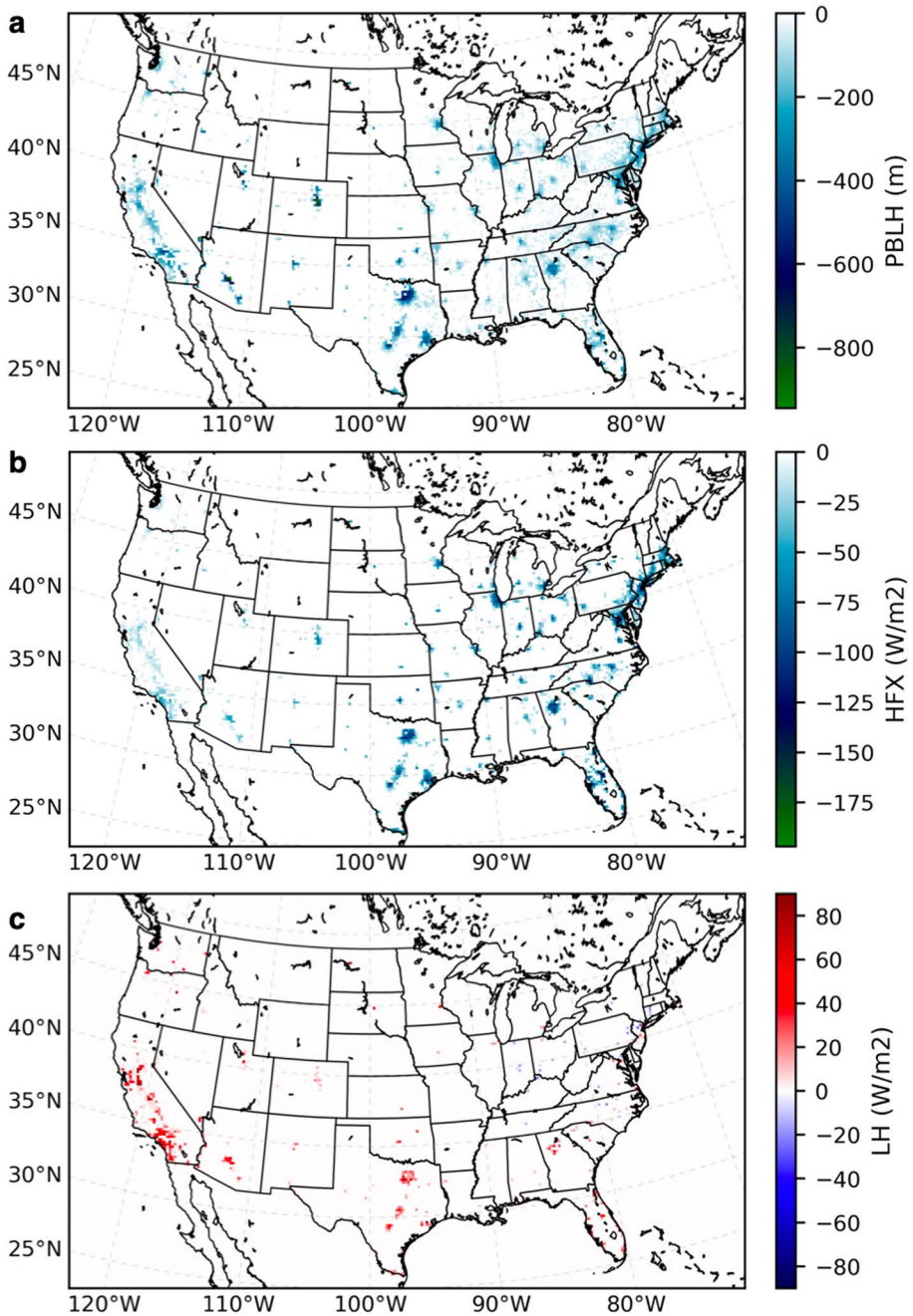

Fig. 4 WRF simulated ten-year averaged summertime (JJA) difference in **a** boundary layer depth, **b** sensible and **c** latent heat flux due to full adaptation implementation on urban development (ICLUS A2 2100) for a projected end of century climate (CESM RCP 8.5 forcing). Results are shown for 14:00 LMST. Full adaptation includes cool roofs, green roofs and street trees simultaneously implemented

exceeding 500 m over southern Great Plains urban regions. The magnitude of UBL height reduction from full adaptation is larger than that induced by cool roof implementation (Fig. 3a), and the spatial extent of full adaptation impacts is greater as well. For example, across mid-Atlantic urban regions, impacts on UBL depth reduction resulting from the full adaptation scenario appear to extend beyond the scale of implementation itself. The major driver of UBL depth reduction is the decrease in sensible heat flux (Fig. 4b). The implementation of the full adaptation strategy also results in increased latent heat fluxes that are more evident across southwestern and Sunbelt cities (Fig. 4c).

3.2 Case study cities

3.2.1 UBL height

We next present a summary of results across a range of metropolitan regions in order to illustrate end-of-century variability in simulated UBL resulting from the combined impacts of greenhouse gas induced climate change, urban

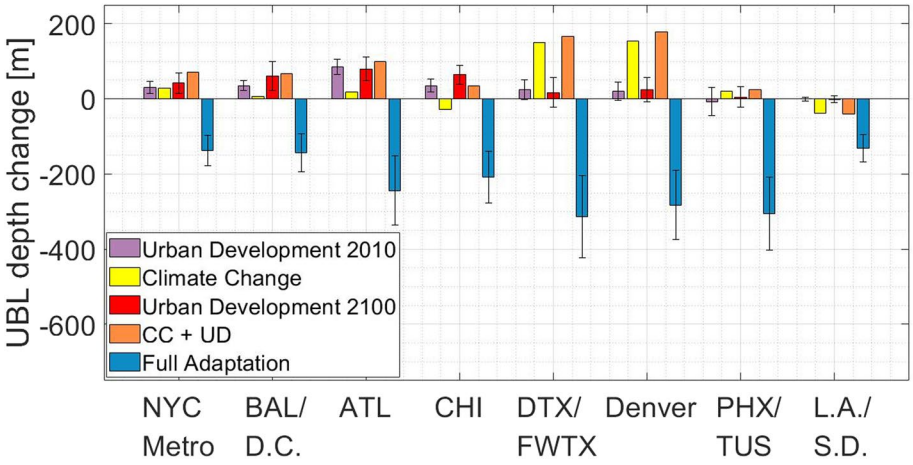

Fig. 5 Summary of WRF simulated ten-year averaged summertime (JJA) UBL impacts for eight US metropolitan areas. Physical drivers responsible for UBL impacts are: purple bars—impact of urban development (UD, ICLUS A2 2100—A2 2010) for a contemporary climate (ECMWF ERA Interim forcing); yellow bars—impact of climate change (CC) only (difference between end and start of century climates); red bars—impact of urban development (UD, ICLUS A2 2100—A2 2010) for a projected end of century climate (CESM RCP 8.5); orange bars—impact of combined urban development and climate change; blue bars—impact of full adaptation on urban development for a projected end of century climate (CESM RCP 8.5). Error bars represent 1σ standard deviation of the 10-year averages. Full adaptation includes cool roofs, green roofs and street trees simultaneously implemented. Results are shown for 14:00 LMST. City acronyms: NYC—New York City; BAL/D.C.—Baltimore/ Washington D.C.; ATL—Atlanta; CHI—Chicago; DTX/FWTX—Dallas/ Fort Worth; PHX/TUS—Phoenix/Tucson; L.A./S.D.—Los Angeles—San Diego

development and heat adaptation strategies. Figure 5 shows the separate and combined impacts of urban development, climate change and full adaptation on JJA UBL depth over the eight case study metro areas at 14:00 LMST. Six of the eight metropolitan regions show that urban development, under both a contemporary (purple bars) and future (red bars) climate, leads to average increases in UBL depth on the order of a few tens of meters. The magnitude of impacts is greater in southeastern metro areas, with average peaks of $\Delta \cong 80$ m over Atlanta. Increases of UBL height maximize at $\Delta \cong 20$ m over the Dallas-Fort Worth and Denver metro areas and become negligible for the Phoenix-Tucson and Los Angeles-San Diego metros, the latter of which show no discernible change in UBL depth with urban development. Figure 5 also shows the impact of climate change (i.e., the difference between start and end-of-century climate; simulation no. 3 minus simulation no. 1, Table 1; yellow bars) on UBL heights of the case study metro areas. We do not present an uncertainty estimate for climate change induced alterations of UBL height (yellow and orange bars in Fig. 5), unlike results highlighting urban development and adaptation strategies. For the latter, standard uncertainty estimates are possible since the simulation period between the samples being compared is identical. In the case of climate change induced alterations of UBL height, the periods/years of simulation that are compared differ, precluding a statistical assessment that is physically meaningful (e.g., through a pairwise comparison of the 2099 UBL to the 2009 UBL). The simulated combined effect of urban development and climate change (simulation no. 4 minus simulation no. 1, Table 1) scales linearly to the sum of climate change and urban development. The combined effects of urban development and climate change lead to an increase in UBL depth for all the examined cities except the Los Angeles/San Diego urban corridor. These results highlight the importance of characterizing projected changes in UBL depth that arise from urban development as well as those arising from large-scale climate change. Consistent with the results of Fig. 4, the implementation of a full adaptation strategy (blue bars) during JJA in a projected end-of-century climate would completely offset the increase in UBL height due to urban development and climate change (orange bars). In all cases, the reduction of UBL height extends to several tens of meters beyond the offset of urban development and climate change impacts. UBL height reductions are projected to be larger over inland urban agglomerations (Atlanta, Chicago, Dallas-Fort Worth and Phoenix-Tucson) and smaller over coastal urban areas (New York, Baltimore-Washington D.C. and Los Angeles-San Diego).

It is instructive to ascertain the individual impacts of each heat adaptation measure on UBL height across the case study metropolitan regions examined. Figure 6 shows a summary of impacts of all considered heat adaptation strategies on JJA UBL heights over the eight case study cities for a projected end-of-century climate at 14:00 LMST. Consistent with previous results (see Fig. 3), the largest reduction in UBL depth is due to cool roofs, while green roofs have the smallest impact in all cities except Atlanta and Denver. The

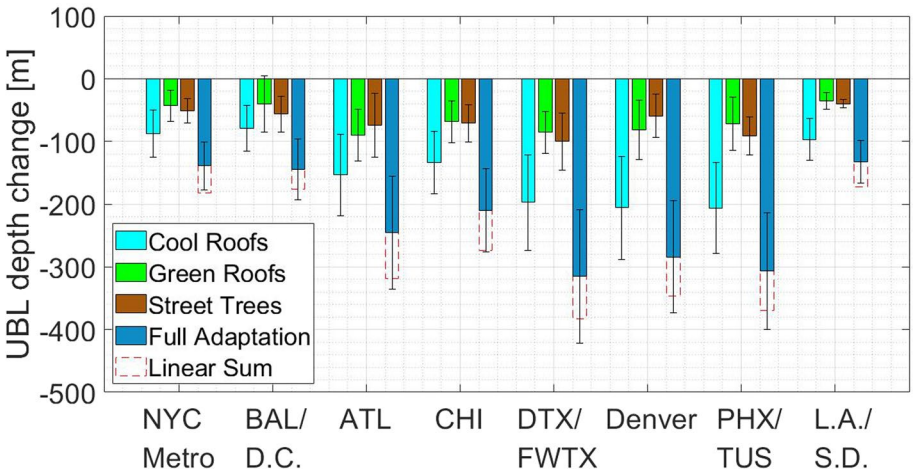

Fig. 6 Summary of WRF simulated ten-year averaged summertime (JJA) UBL impacts for eight US metropolitan areas undergoing urban development (ICLUS A2 2100) for a projected end of century climate (CESM RCP 8.5). Heat adaptation strategies responsible for UBL impacts are: cyan bars—impact of cool roofs; green bars—impact of green roofs; brown bars—impact of street trees; blue bars—impact of full adaptation on urban development for a projected end of century climate (CESM RCP 8.5). Red-dashed transparent bars represent the linear sum of cool roofs, green roofs and street trees impacts. Error bars represent 1σ standard deviation of the 10-year averages. Full adaptation includes cool roofs, green roofs and street trees simultaneously implemented. Results are shown for 14:00 LMST. City acronyms: NYC—New York City; BAL/D.C.—Baltimore/ Washington D.C.; ATL—Atlanta; CHI—Chicago; DTX/FWTX—Dallas/ Fort Worth; PHX/TUS—Phoenix/Tucson; L.A./S.D.—Los Angeles—San Diego

impacts of cool roofs, green roofs and full adaptation show the same pattern as in Fig. 5, namely that of greater reductions of UBL depth over inland urban regions and smaller reductions over coastal urban regions. Street trees induced impacts show, instead, a more geographically uniform effect with a maximum UBL reduction ($\Delta \cong -100$ m) over Dallas-Fort Worth metro and a minimum reduction ($\Delta \cong -40$ m) over Los Angeles-San Diego metro. The impacts from the three individual strategies do not sum linearly in the full adaptation scenario. The simulation of the simultaneous implementation of cool roofs, green roofs, and street trees produces impacts that are on average ~20% smaller than their linear sum, suggesting that impacts from individual strategies may mutually counterbalance.

3.2.2 Analysis of heat fluxes

We next examine annual composites of daily average values of UBL height, sensible and latent heat fluxes to explore seasonal trends in changes of the aforementioned variables over the eight case study metro areas. In accordance with what is shown in Fig. 4 and what was discussed in Sect. 3.1, Fig. 7 shows that the reduction in UBL height is mostly driven by decreases in sensible heat flux (red bars). However, the magnitude of UBL depth reduction is not linearly related to the reduction in sensible heat flux. Full adaptation implementation is projected to increase ground heat flux everywhere across CONUS, and it is projected to increase latent heat flux in southwestern regions (Dallas/Fort Worth, Denver, Phoenix/Tucson, Los Angeles/San Diego). The magnitude of these increases is smaller than the decreases in sensible heat flux everywhere across CONUS. Results from the Los Angeles/San Diego metro areas seem to present an anomaly. There, despite the largest reduction in sensible heat fluxes among the eight case study cities, the reduction in UBL height is the smallest in the sample.

To address this, we next examine the annual evolution of heat fluxes for the Los Angeles/San Diego metro areas. Figure 8 shows ten-year daily averaged (i.e., annual composite) changes in UBL height, sensible and latent heat fluxes due to full adaptation, over the metropolitan areas of Los Angeles and San Diego, in a projected end-of-century climate at 14:00 LMST. Despite the reduction in sensible heat flux (purple dashed line in Fig. 8b), illustrating a clear seasonal trend with a maximum reduction ($\Delta \cong -180$ W/m^2) in mid-July, UBL depth reduction stays constant at $\Delta \cong -100$ m throughout the year (blue dashed line in Fig. 8a). This discrepancy may be explained by a concurrent summer increase in latent heat flux ($\Delta \cong 50$ W/m^2, green dashed line in Fig. 8b), which adds thermal energy to the atmosphere thus reducing its static stability. Figure 9 shows the annual average composite for the New York City metropolitan area as a means of comparison. Here, unlike Los Angeles-San Diego, the change in latent heat fluxes due to full adaptation is small. Despite a three times smaller summertime decrease in sensible heat flux for the New York City (NYC) metropolitan area ($\Delta \cong -60$ W/m^2

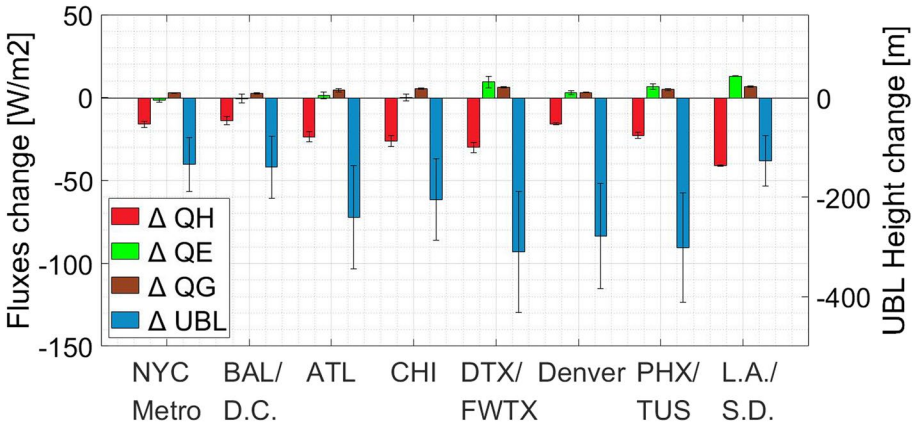

Fig. 7 Summary of WRF simulated ten-year averaged summertime (JJA) full adaptation induced changes in surface energy balance components for eight US metropolitan areas undergoing urban development (ICLUS A2 2100) for a projected end of century climate (CESM RCP 8.5). Physical drivers responsible for full adaptation impacts on UBLs are: red bars—change in sensible heat flux (Δ QH); green bars—change in latent heat flux (Δ QE); brown bars—change in stored heat (Δ QG). Blue bars display the resulting impact of full adaptation on selected UBLs. Error bars represent 1σ standard deviation of the 10-year averages. Full adaptation includes cool roofs, green roofs and street trees simultaneously implemented. Results are shown for 14:00 LMST. City acronyms: NYC—New York City; BAL/D.C.—Baltimore/ Washington D.C.; ATL—Atlanta; CHI—Chicago; DTX/FWTX—Dallas/ Fort Worth; PHX/TUS—Phoenix/Tucson; L.A./S.D.—Los Angeles–San Diego

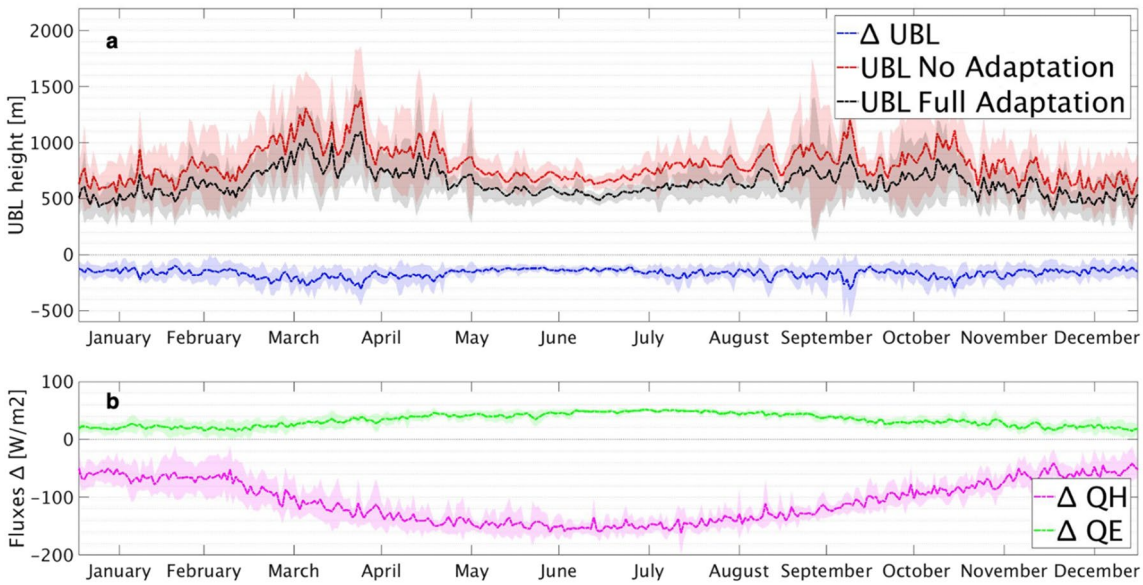

Fig. 8 Annual average composite of **a** UBL depth over the Los Angeles and San Diego metropolitan areas undergoing urban development (ICLUS A2 2100) for a projected end of century climate (CESM RCP 8.5). Red dashed line represents UBL depth for the No Adaptation scenario; black dashed line represents UBL depth for the Full Adaptation scenario; blue dashed line represents their difference (Full Adaptation minus No Adaptation). Plot **b** represents the differences (Full Adaptation minus No Adaptation) in sensible (QH) and latent (QE) heat fluxes due to Full Adaptation implementation. Shades represent 1σ standard deviation about the 10-year average. The time shown is 14:00 LMST. Full adaptation includes cool roofs, green roofs and street trees simultaneously implemented

in July, purple dashed line in Fig. 9b) compared to that shown for Los Angeles and San Diego, the reduction in NYC UBL height is almost twice as large ($\Delta \cong -180$ m in July, blue dashed line in Fig. 9a) as in southern California. These results highlight the importance of considering the modified surface energy balance when evaluating the climatological impacts of heat adaptation measures (see Broadbent et al. 2020b).

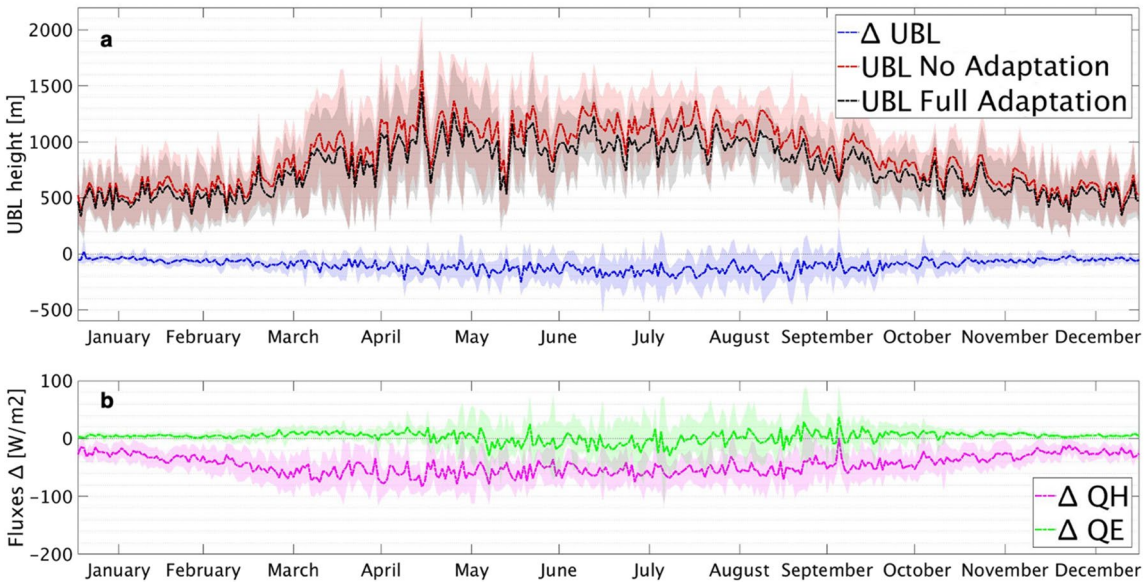

Fig. 9 Annual average composite of **a** UBL depth over the New York metropolitan area undergoing urban development (ICLUS A2 2100) for a projected end of century climate (CESM RCP 8.5). Red dashed line represents UBL depth for the No Adaptation scenario; black dashed line represents UBL depth for the Full Adaptation scenario; blue dashed line represents their difference (Full Adaptation minus No Adaptation). Plot **b** represents the differences (Full Adaptation minus No Adaptation) in sensible (QH, purple dashed line) and latent (QE, green dashed line) heat fluxes due to Full Adaptation implementation. Shades represent 1σ standard deviation about the 10-year average. The time shown is 14:00 LMST. Full adaptation includes cool roofs, green roofs and street trees simultaneously implemented

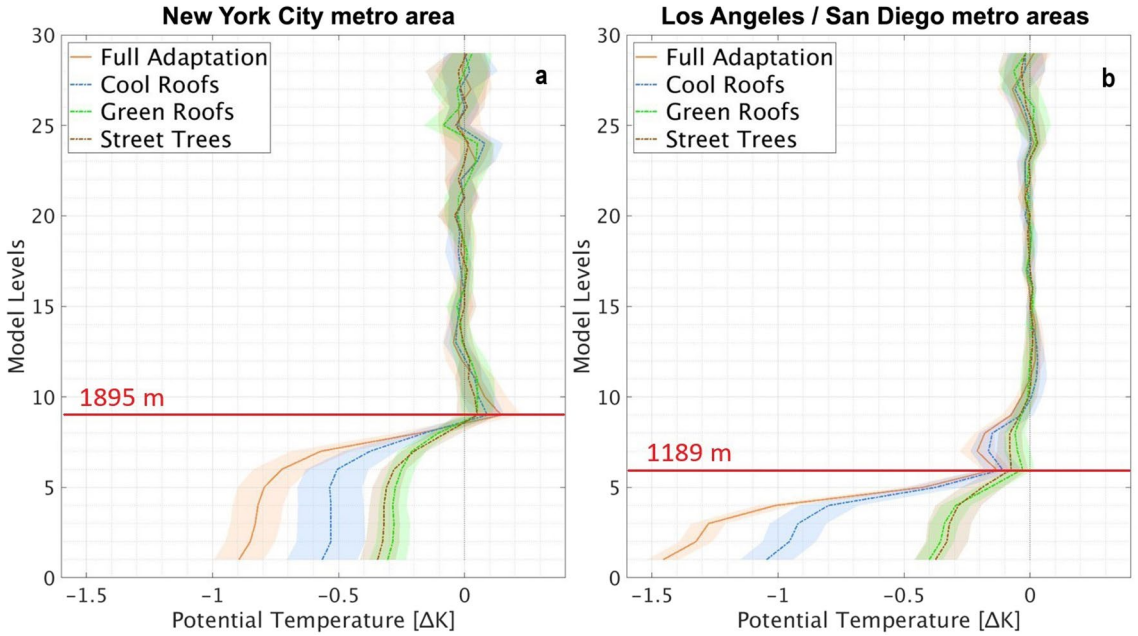

Fig. 10 Ten-year averages of summertime (JJA) potential temperature differences between no adaptation and full adaptation scenarios (Full Adaptation minus No Adaptation) for **a** New York and **b** Los Angeles and San Diego metropolitan areas undergoing urban development (ICLUS A2 2100) for a projected end of century climate (CESM RCP 8.5). Shaded areas represent 1σ standard deviation of the 10-year averages. The time shown is 14:00 LMST. Full adaptation includes cool roofs, green roofs and street trees simultaneously implemented

3.2.3 Static stability

The impact of latent heat flux increase due to heat adaptation strategies is also evident in Fig. 10. Here, ten-year averages of 14:00 (LMST) JJA potential temperature differences between no adaptation (simulation

no. 4, Table 1) and heat adaptation strategies (simulations no. 5–8, Table 1) are presented for the NYC metro-region (Fig. 10a) and Los Angeles and San Diego (Fig. 10b) metro areas. Consistent with the sensible heat flux change shown in Figs. 8b and 9b, the magnitude of potential temperature reduction at the lowest model level due to full adaptation strategies is smaller in New York ($\Delta \cong -0.9$ K, Fig. 10a) than in the Los Angeles and San Diego metro areas ($\Delta \cong -1.43$ K, Fig. 10b). However, the vertical extent of potential temperature reduction is more than 700 m higher over the New York metro-area (red line marker in Fig. 10a) than across the Los Angeles/San Diego corridor (red line marker in Fig. 10b), possibly as a consequence of added moisture from increased latent heat fluxes. Altitudes indicated by red line markers in Fig. 10 are obtained by averaging summertime height of model level 9 (NYC metro) and model level 6 (LA/SD metro) across the 2090–2099 decade. Consistent with the results of heat adaptation impacts on air temperatures (Krayenhoff et al. 2018) and UBL depth (Figs. 3 and 6), the major contribution in terms of potential temperature reduction comes from cool roofs (blue dashed lines in Fig. 10). The impact of full adaptation on potential temperature is smaller than the linear sum of impacts from the individual adaptation strategies (~30% percent smaller in New York, Fig. 10a; ~20% smaller in Los Angeles and San Diego, Fig. 10b). Similar impacts on daytime potential temperature are found for all other case study metropolitan areas.

The decreasing impact of full adaptation strategies on potential temperature lapse rates persists throughout the nighttime, reinforcing the static stability of the nocturnal boundary layer for all eight case study metro areas affected by urban development (ICLUS 2100) for a projected end-of-century summertime climate (CESM 2100). Increases in static stability are greater for cities characterized by more humid background climates, with peak nocturnal reduction over the Dallas/Fort Worth metro areas ($\Delta \cong -1.1$ K, Fig. 11), and reduced impacts over more arid metro areas with minimum impact over the Los Angeles and San Diego metro areas ($\Delta \cong -0.2$ K, Fig. 11).

3.2.4 Vertical winds

The impact of heat adaptation strategies on UBL depth and potential temperature lapse rates extends to regional-scale dynamics and vertical wind profiles. The implementation of heat adaptation strategies reduces the magnitude of vertical winds, with peak reductions due to full adaptation ranging from $\Delta \cong -0.006$ m/s in the New York metro-region to $\Delta \cong -0.045$ m/s over the Phoenix-Tucson metro areas. Consistent with the impact on all other meteorological parameters analyzed, the greatest impact on vertical winds arises from cool roof deployment. In all case study cities, except Denver, heat adaptation strategies promote stronger subsidence through most of the UBL. In the semi-arid regions of the south and southwest this reversal effect becomes considerably intense, reaching downward speeds of $w < -0.05$ m/s at the top of the summertime boundary layer ($h \cong 3000$ m) over the Phoenix and Tucson metro areas (Fig. 12). Figure 12 shows the same pattern of impacts as was previously presented in Figs. 6 and 10. The most effective individual heat adaptation strategy in reducing vertical winds are cool roofs, and the impact due to full adaptation is smaller than the linear sum of individual impacts (~40% smaller over Phoenix and Tucson metro areas).

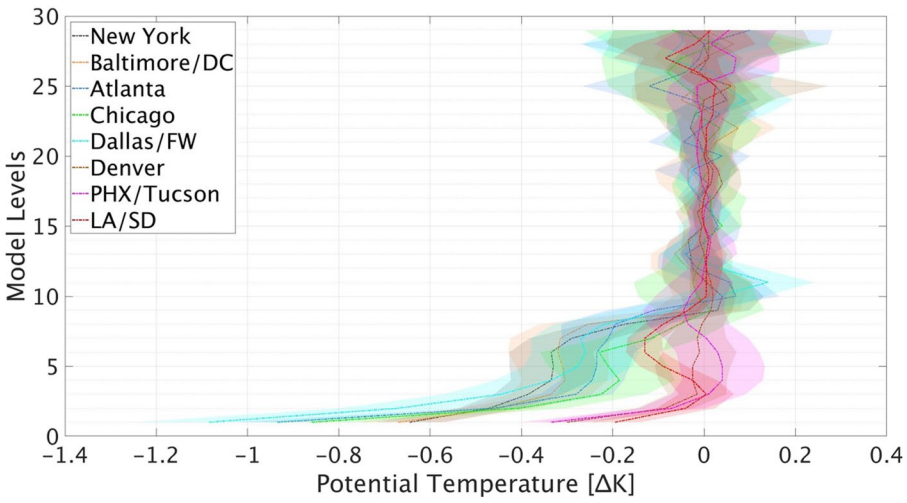

Fig. 11 Ten-year averages of summertime (JJA) potential temperature differences between no adaptation and full adaptation scenarios (Full Adaptation minus No Adaptation) for all case study metropolitan areas undergoing urban development (ICLUS A2 2100) for a projected end of century climate (CESM RCP 8.5). The time shown is 02:00 LMST. Shaded areas represent 1σ standard deviation of the 10-year averages. Full adaptation includes cool roofs, green roofs and street trees simultaneously implemented

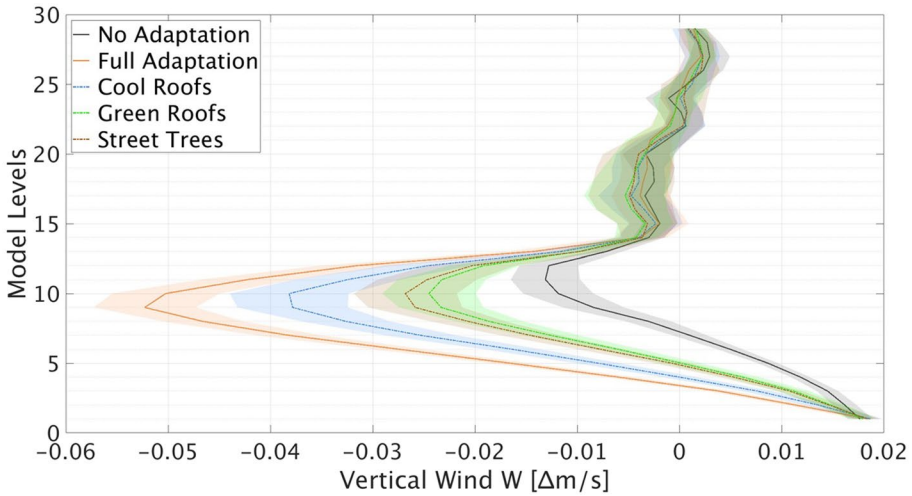

Fig. 12 Ten-year averages of seasonal vertical wind speed changes due to Full Adaptation implementation over the Phoenix and Tucson metropolitan areas undergoing urban development for a projected end of century climate (CESM RCP 8.5). Black line represents vertical wind profiles in a No-Adaptation scenario. Orange line represents vertical wind profiles in a Full Adaptation scenario. Dashed lines represent vertical wind profiles for each individual adaptation strategy: blue line represents the impact of cool roofs implementation; green line represents the impact of green roofs implementation; brown line represents the impact of street trees implementation. Shaded areas represent 1σ standard deviation of the 10-year averages. The time shown is 14:00 LMST. Full adaptation includes cool roofs, green roofs and street trees simultaneously implemented

4 Discussion and conclusions

4.1 Summary of findings

Individual and combined impacts of climate change, urban development, and heat adaptation strategies on UBL depth and structure over urban regions across CONUS have been examined using a set of decadal 20 km grid spacing WRF simulations for both start and end of twenty-first century climate and urbanization scenarios. Eight case study metropolitan areas have been selected for further analysis and comparison of impacts. The results presented in this paper show that urban development (ICLUS 2100) and a high intensity greenhouse gas emissions scenario (RCP 8.5) are expected to increase UBL height across conterminous US conurbations within a projected end-of-century climate. Urban development UBL height effects are greater in the eastern portion of the country but are reduced across western municipalities. This is probably because in the eastern regions urban development more frequently replaces previously existing vegetation, resulting in greater latent heat flux decreases. Heat adaptation strategies, and cool roofs in particular, are expected to completely offset the combined effect of urban development and climate change on UBL depth and produce a further height reduction of a few hundred meters. Heat adaptation impacts on UBL depth in the cities of a projected end-of-century CONUS are weaker over coastal areas and stronger inland. UBL height reduction is the consequence of a modified urban surface energy balance, specifically, reduced sensible heat fluxes. In one of the examined urban regions, across southern California, our imposed full heat adaptation induced an increase in latent heat flux that may counterbalance the height decreasing adaptation effect on UBL depth. However, this result appears to be specific to the Los Angeles/San Diego metropolitan region and requires further examination. Heat adaptation induced modifications to urban landscapes are expected to increase static stability near the surface, during both daytime and nighttime, and induce subsidence across the UBL. Importantly, the combined impacts on UBL depth, static stability and vertical winds of all adaptation strategies simultaneously applied (i.e., full adaptation) are always smaller than the linear sum of individual impacts.

4.2 Discussion of results

The reduction of UBL depth and convective mixing may have important consequences on air quality, as it reduces the volume of air available for pollutant dilution and dispersion. That is especially true near the surface where most human activities take place. For example, assuming no change in particulate matter emissions, increased daytime and nighttime static stability and associated subsidence can increase pollutant concentrations at pedestrian level. The reduction of vertical transport of moisture associated with cool roof implementation can also be detrimental to cloud formation processes, and consequently reduce the amount of precipitation in urban areas or their downwind environments

(Marshall Shepherd 2005; Kishtawal et al. 2010; Georgescu et al. 2021). This hypothesis, which requires further investigation, may contribute to further exacerbate air quality deterioration by reducing the efficacy of rain-based removal of atmospheric pollutants. Since adaptation measures can change boundary layer height and structure, it is important that the potential implications of adaptation measures on air quality and precipitation be weighed against cooling benefits. The presented case of the dynamics over the Los Angeles and San Diego metro areas is a prime example. In this example, full adaptation induced increases in latent heat flux attenuates the UBL depth reduction driven by the largest decrease in sensible heat flux among the case study cities, as adding moisture from evapotranspiration processes of green roofs and street trees to the lower atmosphere contributes to reducing its static stability. However, a comparable increase in latent heat fluxes in the Dallas/Fort Worth metro areas does not produce a similar counterbalancing effect, suggesting that other potential contributors (e.g., ocean-land circulation) may play a role in Southern California. The role of adaptation induced increases in moisture upon UBL height changes needs further investigation, especially because increased humidity at the surface level negatively affects human outdoor thermal comfort (Masterton and Richardson 1979), thus jeopardizing a major objective of heat adaptation strategies. Furthermore, the expected nighttime increase in static stability induced by heat adaptation strategies in cities characterized by more humid background climates demonstrate the need for careful consideration of environmental tradeoffs. This study helps inform the discussion surrounding the diverse impacts associated with heat adaptation in urban environments and supports continued efforts focused on development of increasingly resilient future cities that preserve the health of their dwellers.

4.3 Discussion of limitations

We focused our analysis on the magnitude of decadal averaged summertime impacts. No assessment has been made on the magnitude of impacts during extreme events such as heat waves, nor any estimation of impacts on duration and frequency of said events has been assessed. Reduced convection and vertical transport of moisture may reduce cloud formation; however, the dynamical balance between increases of surface albedo due to cool roof implementation and decreases in atmospheric albedo due to cloud cover reduction has not been considered here.

Longwave radiation exchange by street trees has a modest impact on the pedestrian level thermal environment at night (e.g., see Krayenhoff et al. 2020). There is no evidence (that we are aware of) that longwave exchange by urban trees has a substantive impact during daytime, or on the boundary-layer above, and it is very unlikely that this process impacts the daytime UBL depth. We do not expect morphological features of trees to have a sizeable effect on our daytime results. Tree foliage is assumed to be randomly distributed (accounting for between-crown clumping—see Krayenhoff et al. 2014) within the urban canyon space between the heights of 2.5 m and 7.5 m. Canyon mean LAI is 2.0 m^2 m^{-2}. Trees that are taller than buildings (5 m tall for 2 of 3 urban zones) provide some shade to building roofs, reducing average roof surface sensible heat flux and associated buoyancy production. Shorter (taller) trees would be expected to impact UBL depth to a smaller (greater) degree.

Modifications of landscape characteristics can alter the patterns of wind convergence and divergence near the surface (Pielke 2001). Preliminary analysis of our results shows that heat adaptation strategies may alter horizontal wind circulation patterns within and downwind of cities. However, higher resolution simulations are required to substantiate such assessment with acceptable confidence. In addition, WRF version 3.6.1 accepts only three urban categories by default (low-intensity residential, high-intensity residential, and industrial and commercial; Chen et al. 2011), thus limiting the resolution of urban land use and land cover representation (note that such datasets, with more urban categories, exist for contemporary climate, but are not available for projected, future, climates). Similar considerations exist regarding the absence of a building energy model or parameterization (BEM and BEP, respectively), which our simulations have accounted for with a parameterized anthropogenic heat flux.

The use of fixed parameters across the entire CONUS to represent three-dimensional urban characteristics (e.g., building and tree heights and urban canyon aspect ratios) likely minimizes variability of morphological parameters and roughness lengths within and between CONUS cities. Burian et al. (2002) used a GIS approach to compute building height statistics for three U.S. cities and found differences in average ($\Delta h = 6.4$ m) and maximum ($\Delta h = 194$ m) building heights for the cities of Los Angeles and Phoenix. Ellefsen (1991) used direct measurement to retrieve information on height and wall surface areas and construction materials of ten U.S. cities and found regional differences. For example, at the time of measurements, combined wall and roof areas of downtown Atlanta (323 hectares) was almost ten times greater than the corresponding building surfaces in Baltimore (36 hectares, Ellefsen 1991). The morphology of built areas in urban environments has a strong impact on surface drag and heat trapping in urban canyons. That in turn affects the modeling of shear and buoyancy induced turbulence that contributes to the determination of UBL depth in the YSU PBL scheme used in the simulations. An increase in urban development, in addition to increased sensible heat

flux, is expected to increase urban roughness and shear turbulence production. That is especially relevant in the Southwest where the lack of forests increases the difference in aerodynamic resistance between urban and non-urban areas. However, the increase in UBL depth due to urban expansion alone (Fig. 5, purple and red bars) is one order of magnitude smaller than the UBL depth reduction due to full adaptation (Fig. 5, blue bars). We assume the change in surface heat fluxes to be the dominant physical process impacting the projected climatology of UBLs across CONUS.

Future research addressing these aspects with convection resolving, high-resolution coupled atmosphere-chemistry simulations will help provide a better and more complete assessment of the climatology of the UBL in light of climate change, urban development and heat adaptation.

Acknowledgements This work was supported by National Science Foundation Sustainability Research Network Cooperative Agreement 1444758, the Urban Water Innovation Network (UWIN). The authors acknowledge the large-scale, high-performance and high-throughput computing support from Research Computing at Arizona State University.

Funding National Science Foundation Sustainability Research Network Cooperative Agreement 1444758, the Urban Water Innovation Network (UWIN).

Availability of data and material Data is available from the lead/corresponding author upon reasonable request.

Code availability Analysis MATLAB codes available upon request.

Declarations

Conflicts of interest The authors declare to have no conflict of interest connected with the presented research.

References

Akbari H, Matthews HD (2012) Global cooling updates: reflective roofs and pavements. Energy Build 55:2–6

Aleksandrowicz O, Vuckovic M, Kiesel K, Mahdavi A (2017) Current trends in urban heat island mitigation research: observations based on a comprehensive research repository. Urban Clim 21:1–26

Barlow JF (2014) Progress in observing and modelling the urban boundary layer. Urban Climate 10:216–240

Bass B, Krayenhoff ES, Martilli A, Stull RB, Auld H (2003) The impact of green roofs on Toronto's urban heat island. In: Proceedings of Greening Rooftops for Sustainable Communities

Berrisford P, Dee DP, Poli P, Brugge R, Fielding M, Fuentes M, Kållberg PW, Kobayashi S, Uppala S, Simmons A (2011) The ERA-Interim archive, version 2.0

Bierwagen BG et al (2010) National housing and impervious surface scenarios for integrated climate impact assessments. Proc Natl Acad Sci USA 107:20887–20892

Broadbent AM, Krayenhoff ES, Georgescu M (2020a) The motley drivers of heat and cold exposure in 21st century US cities. In: Proceedings of the National Academies of Sciences (USA), Accepted

Broadbent AM, Krayenhoff ES, Georgescu M (2020b) Efficacy of cool roofs at reducing pedestrian-level air temperature during projected 21st century heatwaves in Atlanta, Detroit, and Phoenix (USA). Environ Res Lett

Bruinsel L (2020) Urban heat adaptation. Understanding the emergence of institutional barriers for heat adaptation

Burian SJ, Brown MJ, Velugubantla SP (2002) Building height-characteristics in three US cities (No. LA-UR-02-1089). Los Alamos National Laboratory

Cao Q, Yu D, Georgescu M, Wu J, Wang W (2018) Impacts of future urban expansion on summer climate and heat-related human health in eastern China. Environ Int 112:134–146

Census Bureau Regions and Divisions with State FIPS Codes. https://www2.census.gov/geo/pdfs/maps-data/maps/reference/us_regdiv.pdf. Accessed: 13 July 2020

Chen Y, Zhang N (2018) Urban Heat Island Mitigation Effectiveness under Extreme Heat Conditions in the Suzhou–Wuxi–Changzhou Metropolitan Area, China. J Appl Meteorol Climatol 57(2):235–253

Chen F et al (2011) The integrated WRF/urban modelling system: development, evaluation, and applications to urban environmental problems. Int J Climatol 31:273–288

Costanzo V, Evola G, Marletta L (2016) Energy savings in buildings or UHI mitigation? Comparison between green roofs and cool roofs. Energy Build 114:247–255

Ellefsen R (1991) Mapping and measuring buildings in the canopy boundary layer in ten U.S. cities. Energy Build 16(3–4):1025–1049

ENERGY STAR Roof Product List (Energy Star, 2013); https://go.nature.com/2CuhGPn

Georgescu M (2015) Challenges associated with adaptation to future urban expansion. J Clim 28(7):2544–2563

Georgescu M, Morefield PE, Bierwagen BG, Weaver CP (2014) Urban adaptation can roll back warming of emerging megapolitan regions. Proc Natl Acad Sci 111(8):2909–2914

Georgescu M, Broadbent AM, Wang M, Krayenhoff ES, Moustaoui M (2021) Precipitation response to climate change and urban development over the continental United States. Environ Res Lett 16(4):044001. https://iopscience.iop.org/article/10.1088/1748-9326/abd8ac/meta

Gilbert H, Mandel BH, Levinson R (2016) Keeping California cool: recent cool community developments. Energy Build 114:20–26

Gillner S, Vogt J, Tharang A, Dettmann S, Roloff A (2015) Role of street trees in mitigating effects of heat and drought at highly sealed urban sites. Landsc Urban Plan 143:33–42

Hong SY, Pan HL (1996) Nonlocal boundary layer vertical diffusion in a medium-range forecast model. Mon Weather Rev 124(10):2322–2339

Hong SY, Noh Y, Dudhia J (2006) A new vertical diffusion package with an explicit treatment of entrainment processes. Mon Weather Rev 134(9):2318–2341

IPCC (2014): Annex II: Glossary [Agard, J., E.L.F. Schipper, J. Birkmann, M. Campos, C. Dubeux, Y. Nojiri, L. Olsson, B. Osman-Elasha, M. Pelling, M.J. Prather, M.G. Rivera-Ferre, O.C. Ruppel, A. Sallenger, K.R. Smith, A.L. St. Clair, K.J. Mach, M.D. Mastrandrea, and T.E. Bilir (eds.)]. In: Climate Change 2014: Impacts, Adaptation, and Vulnerability. Part B: Regional Aspects. Contribution of Working Group II to the Fifth Assessment Report of the Intergovernmental Panel on Climate Change [Barros, V.R., C.B. Field, D.J. Dokken, M.D. Mastrandrea, K.J. Mach, T.E. Bilir, M. Chatterjee, K.L. Ebi, Y.O. Estrada, R.C. Genova, B. Girma, E.S. Kissel, A.N. Levy, S. MacCracken, P.R. Mastrandrea, and L.L. White (eds.)]. Cambridge University Press, Cambridge, United Kingdom and New York, NY, USA, pp. 1757–1776

Kishtawal CM, Niyogi D, Tewari M, Pielke RA Sr, Shepherd JM (2010) Urbanization signature in the observed heavy rainfall climatology over India. Int J Climatol 30(13):1908–1916

Krayenhoff ES, Christen A, Martilli A, Oke TR (2014) A multi-layer radiation model for urban neighbourhoods with trees. Bound-Layer Meteorol 151(1):139–178

Krayenhoff ES, Moustaoui M, Broadbent AM, Gupta V, Georgescu M (2018) Diurnal interaction between urban expansion, climate change and adaptation in US cities. Nat Clim Change 8(12):1097–1103

Krayenhoff ES, Jiang T, Christen A, Martilli A, Oke TR, Bailey BN, Nazarian N, Voogt JA, Giometto M, Stastny A, Crawford B (2020) A multi-layer urban canopy meteorological model with trees (BEP-Tree): street tree impacts on pedestrian-level climate. Urban Clim 32:100590

Krayenhoff ES, Broadbent AM, Zhao L, Georgescu M, Middel A, Voogt JA, Martilli A, Sailor DJ, Erell E (2021) Cooling hot cities: a systematic and critical review of the numerical modelling literature. Environ Res Lett

Kusaka H, Kimura F (2004) Coupling a single-layer urban canopy model with a simple atmospheric model: Impact on urban heat island simulation for an idealized case. J Meteorol Soc Japan. Ser. II 82(1):67–80

Kusaka H, Kondo H, Kikegawa Y, Kimura F (2001) A simple single-layer urban canopy model for atmospheric models: comparison with multi-layer and slab models. Bound Layer Meteorol 101:329–358

Marshall Shepherd JM (2005) A review of current investigations of urban-induced rainfall and recommendations for the future. Earth Interact 9(12):1–27. https://doi.org/10.1175/EI156.1

Masterton JM, Richardson FA (1979) Humidex: a method of quantifying human discomfort due to excessive heat and humidity. Environment Canada, Atmospheric Environment

Meehl GA, Tebaldi C (2004) More intense, more frequent, and longer lasting heat waves in the 21st century. Science 305(5686):994–997

Monaghan AJ, Steinhoff DF, Bruyere CL, Yates D (2014) NCAR CESM global bias-corrected CMIP5 output to support WRF/MPAS research. In: Research Data Archive at the National Center for Atmospheric Research, Computational and Information Systems Laboratory, Boulder, Colo. Accessed, 25(03), 2018

Narita KI, Sugawara H, Honjo T (2008) Effects of roadside trees on the thermal environment within a street canyon. Geogr Rep Tokyo Metrop Univ 43:41–48

Noh Y, Cheon WG, Hong SY, Raasch S (2003) Improvement of the K-profile model for the planetary boundary layer based on large eddy simulation data. Bound-Layer Meteorol 107(2):401–427

Oke TR (1982) The energetic basis of the urban heat island. Q J R Meteorol Soc 108(455):1–24

Pielke RA Sr (2001) Influence of the spatial distribution of vegetation and soils on the prediction of cumulus convective rainfall. Rev Geophys 39(2):151–177

Pielke RA, Avissar R (1990) Influence of landscape structure on local and regional climate. Landscape Ecol 4(2–3):133–155

Sailor DJ (1995) Simulated urban climate response to modifications in surface albedo and vegetative cover. J Appl Meteorol 34(7):1694–1704

Seibert P, Beyrich F, Gryning SE, Joffre S, Rasmussen A, Tercier P (2000) Review and intercomparison of operational methods for the determination of the mixing height. Atmos Environ 34(7):1001–1027

Seidel DJ, Zhang Y, Beljaars A, Golaz JC, Jacobson AR, Medeiros B (2012) Climatology of the planetary boundary layer over the continental United States and Europe. J Geophys Res Atmos 117(D17)

Sharma A, Conry P, Fernando HJS, Hamlet AF, Hellmann JJ, Chen F (2016) Green and cool roofs to mitigate urban heat island effects in the Chicago metropolitan area: evaluation with a regional climate model. Environ Res Lett 11(6):064004

Skamarock WC, Klemp JB, Dudhia J, Gill DO, Barker D, Duda MG, Powers JG (2008) A Description of the Advanced Research WRF Version 3 (No. NCAR/TN-475+STR). University Corporation for Atmospheric Research. https://doi.org/10.5065/D68S4MVH

Solomon S (2007) IPCC (2007): climate change the physical science basis. AGUFM 2007:U43D – U51

Song J, Wang ZH (2016) Diurnal changes in urban boundary layer environment induced by urban greening. Environ Res Lett 11(11):114018

Song J, Wang ZH, Wang C (2018) The regional impact of urban heat mitigation strategies on planetary boundary layer dynamics over a semiarid city. J Geophys Res Atmos 123(12):6410–6422

Stull RB (2012) An introduction to boundary layer meteorology (Vol. 13). Springer Science & Business Media

Synnefa A, Dandou A, Santamouris M, Tombrou M, Soulakellis N (2008) On the use of cool materials as a heat island mitigation strategy. J Appl Meteorol Climatol 47(11):2846–2856

Tewari M, Chen F, Wang W, Dudhia J, LeMone MA, Mitchell K, Ek M, Gayno G, Wegiel J, Cuenca RH (2004) Implementation and verification of the unified NOAH land surface model in the WRF model. In: 20th conference on weather analysis and forecasting/16th conference on numerical weather prediction, pp. 11–15.

U.S. EPA (2010) Integrated Climate and Land-Use Scenarios (Iclus) V1.3 User's manual: arcgis tools and datasets for modeling US housing density growth. U.S. Environmental Protection Agency, Washington, DC

Von Storch H, Zwiers FW (2001) Statistical analysis in climate research. Cambridge University Press, Cambridge

Wang C, Wang ZH, Wang C, Myint SW (2019) Environmental cooling provided by urban trees under extreme heat and cold waves in US cities. Remote Sens Environ 227:28–43

Weaver CP, Avissar R (2001) Atmospheric disturbances caused by human modification of the landscape. Bull Am Meteorol Soc 82(2):269–282

Xue Y, Janjic Z, Dudhia J, Vasic R, De Sales F (2014) A review on regional dynamical downscaling in intraseasonal to seasonal simulation/prediction and major factors that affect downscaling ability. Atmos Res 147:68–85

Zhang N, Chen Y, Luo L, Wang Y (2017) Effectiveness of different Urban heat Island mitigation methods and their regional impacts. J Hydrometeorol 18(11):2991–3012. https://doi.org/10.1175/jhm-d-17-0049.1

Zhang C, Wang Y, Xue M (2020) Evaluation of an E─ϵ and three other boundary layer parameterization schemes in the WRF model over the Southeast Pacific and the Southern Great Plains. MWRv 148(3):1121–1145

Zilitinkevich SS (2012) The height of the atmospheric planetary boundary layer: State of the art and new development. National security and human health implications of climate change. Springer, Dordrecht, pp 147–161